ATLAS NOTE

ATLAS-CONF-2013-060

June 21, 2013
Minor revision: June 27, 2013

Search for pair production of a heavy top-like quark decaying to a high-p_{T} W boson and a b quark in the lepton plus jets final state in pp collisions at $\sqrt{s}$ = 8 TeV with the ATLAS detector

The ATLAS Collaboration

Abstract

A search is presented for production of a heavy top-like quark (T) together with its antiparticle, assuming a significant branching ratio for subsequent decay into a W boson and a b quark. The search is based on 14.3 fb^{-1} of pp collisions at $\sqrt{s}$ = 8 TeV recorded in 2012 with the ATLAS detector at the CERN Large Hadron Collider. Data are analysed in the lepton+jets final state, characterised by a high-transverse-momentum isolated electron or muon, large missing transverse momentum and at least four jets, with at least one of them b tagged. The analysis strategy relies on the substantial boost of the W bosons in the $T\bar{T}$ signal when $m_T \gtrsim 400$ GeV. No significant excess of events above the Standard Model expectation is observed. For a chiral fourth generation quark, and under the assumption of a branching ratio $BR(T \to Wb) = 1$, a mass lower than 740 GeV is excluded at 95% CL. For vector-like T quarks, and under the assumption that only the $T \to Wb$, $T \to Zt$ and $T \to Ht$ decay modes contribute, 95% CL upper limits are derived for various masses in the two-dimensional plane of $BR(T \to Wb)$ versus $BR(T \to Ht)$, where H is the Standard Model Higgs boson. These limits are significantly improved by combining this search with a previous search for $T\bar{T} \to Ht + X$, with $H \to b\bar{b}$.

Minor correction in label of Figure 9 with respect to the version of June 21, 2013

1 Introduction

Since the discovery of the top quark [1,2], which completed the third generation of fundamental fermions in the quark sector of the Standard Model (SM) of particle physics, searches for heavier quarks have been of particular interest in high energy physics research. These quarks are often present in new physics models aimed at solving some of the limitations of the SM. Models with an extra family of heavy chiral fermions [3, 4] have been a prominent example for many years. In particular, these models can accommodate new sources of CP violation that could explain the matter-antimatter asymmetry in the universe. In the quark sector, the new weak-isospin doublet contains heavy up-type (T) and down-type (B) quarks which are nearly degenerate in mass [5] and mix with the lighter quarks via an extended CKM matrix. Based on the mixing pattern of the known quarks, it is natural to expect the mixing with third-generation quarks to fdominate and thus that $T \to Wb$ and $B \to Wt$ decays occur with nearly 100% branching ratio. The observation of a new scalar boson by the ATLAS [6] and CMS [7] Collaborations with a mass of ~126 GeV and couplings close to those expected for the SM Higgs boson severely constrains minimal perturbative fourth-generation models [5, 8, 9]. Despite being disfavored, the feature of dominant charged-current decays, also present in other extensions of the SM involving exotic heavy quarks, still make them useful benchmarks in the experimental searches.

Currently, a more compelling possibility is the addition of weak-isospin singlets, doublets or triplets of vector-like quarks [10], defined as quarks for which both chiralities have the same transformation properties under the electroweak group $SU(2) \times U(1)$. Vector-like quarks appear in many extensions of the SM such as little Higgs [11–13] or extra-dimensional models [14, 15]. In these models, a top-partner quark, for simplicity referred to here as T, often plays a key role in cancelling the quadratic divergences in the Higgs boson mass induced by radiative corrections involving the top quark. Therefore, vector-like quarks are expected to mix preferentially with third generation and as a result they present a rich phenomenology. Under this assumption, a vector-like T quark has *a priori* three possible decay modes, $T \to Wb$, $T \to Zt$, and $T \to Ht$, with branching ratios that depend on m_T and the weak-isospin quantum number of the T quark. While all three decay modes can be sizable for a weak-isospin singlet T quark with electric charge of $2/3$, decays to only Zt and Ht are most natural for a doublet T quark. In contrast, a doublet Y quark (following the naming convention in Ref. [10]) with charge $-4/3$ would decay exclusively into W^-b, giving a signature experimentally indistinguishable from that of a chiral fourth-generation T quark[1]. In the case of a triplet, the T quark can decay either as a singlet or a doublet depending on its hypercharge. The observation of a SM-like Higgs boson raises the level of interest in vector-like quark searches, as $T \to Ht$ and $B \to Hb$ decays now have completely specified final states. In addition, it has been pointed out [16–18] that the mixing of the b quark with a B quark, the isospin partner of the Y quark, with mass as low as 700 GeV, could explain the anomalies in the A_{FB}^b and R_b observables in $Z \to b\bar{b}$ at LEP. This provides additional motivation to search for, not only the B quark, but also the Y quark.

The large centre-of-mass energy ($\sqrt{s}$) and integrated luminosity in proton-proton (pp) collisions produced at the CERN Large Hadron Collider (LHC) offer a unique opportunity to probe these models. At the LHC, these exotic heavy quarks would be produced predominantly in pairs via the strong interaction for masses below O(1 TeV) [10], with sizable cross sections and clean experimental signatures.

Most searches for $T\bar{T}$ production by the ATLAS and CMS collaborations using pp collision data at $\sqrt{s} = 7$ TeV focused on the $T \to Wb$ decay mode, exploiting both the lepton+jets signature [19, 20], where one of the W bosons decays leptonically and the other hadronically, and the dilepton signature [21, 22], where both W bosons decay leptonically. These searches make the assumption that $BR(T \to Wb) = 1$, which is reasonable for a chiral fourth generation T quark, but unrealistic in general in the case of vector-like quark models. Under this assumption, the most restrictive lower limit obtained on the mass

[1] Information on b jet charge is not yet being used in these experimental searches.

of a T quark is $m_T > 656$ GeV at 95% confidence level (CL) [19]. The CMS Collaboration has also used the lepton+jets signature to search for the $T \to Zt$ decay mode, also under the assumption that $BR(T \to Zt) = 1$ [23]. The limits derived by these searches can not easily be applied to other branching ratio values, due to the potentially large expected signal contamination from mixed decay modes. A consistent treatment of those additional signal contributions is thus necessary to set quasi-model independent limits on the plane of $BR(T \to Ht)$ vs $BR(T \to Wb)$ as a function of m_T. The branching ratio $BR(T \to Zt)$ is fixed by the assumption that $BR(T \to Zt) = 1 - BR(T \to Wb) - BR(T \to Ht)$. Such an analysis was done by the ATLAS Collaboration [19] using a search for $T\bar{T} \to WbWb$ at $\sqrt{s} = 7$ TeV [19]. More recently, a search for $T\bar{T} \to Ht + X$, with $H \to b\bar{b}$, was performed by the ATLAS Collaboration [24] using 14.3 fb^{-1} of data at $\sqrt{s} = 8$ TeV. This search was particularly sensitive to T quark decays with large branching ratio to Ht and set the most restrictive limits to date on the plane of $BR(T \to Ht)$ vs $BR(T \to Wb)$ as a function of m_T. In particular, under the branching ratio assumptions corresponding to a weak-isospin doublet (singlet) scenario, a T quark with mass lower than 790 (640) GeV was excluded at the 95% confidence level.

In this note a search is presented for $T\bar{T}$ production using 14.3 fb^{-1} of pp collision data at $\sqrt{s} = 8$ TeV collected with the ATLAS detector. The search is optimized for T quark decays with large branching ratio to Wb, thus being complementary to that in Ref. [24]. Events are selected in the lepton+jets channel, requiring a high transverse momentum isolated electron or muon, large missing transverse momentum and at least four jets. Following the strategy advocated in Refs. [25–27], and implemented in Ref. [19], further background suppression is achieved by making additional kinematic requirements that exploit the distinct topology of signal events, which involve W bosons with substantial boost. The result of the search is interpreted both in the context of a chiral fourth-generation T quark, as well as more generically in the context of vector-like quark models.

This note is organised as follows. After a brief overview of the ATLAS detector in Section 2, the main physics objects used in this search, as well as the dataset and event preselection requirements made are discussed in Sections 3 and 4, respectively. Section 5 summarises the simulated samples used for signal and backgrounds, while Section 6 is devoted to the background predictions based on data-driven techniques. The final event selection is presented in Section 7 and the procedure to reconstruct the mass of the T quark, which is the final discriminating variable used in this search, is given in Section 8. A discussion of the systematic uncertainties considered in this search is given in Section 9. The statistical analysis and results obtained are presented in Sections 10 and 11, respectively. Finally, a summary is given in Section 12.

2 ATLAS Detector

The ATLAS detector [28] consists of the following main subsystems: an inner tracking system surrounded by a superconducting solenoid, electromagnetic and hadronic calorimeters, and a muon spectrometer. The inner detector provides tracking information from pixel and silicon microstrip detectors in the pseudorapidity[2] range $|\eta| < 2.5$ and from a transition radiation tracker covering $|\eta| < 2.0$, all immersed in a 2 T magnetic field provided by a superconducting solenoid. The electromagnetic (EM) sampling calorimeter uses lead and liquid-argon (LAr) and is divided into barrel ($|\eta| < 1.475$) and endcap ($1.375 < |\eta| < 3.2$) regions. Hadron calorimetry is based on two different detector technologies,

[2]ATLAS uses a right-handed coordinate system with its origin at the nominal interaction point (IP) in the centre of the detector and the z-axis coinciding with the axis of the beam pipe. The x-axis points from the IP to the centre of the LHC ring, and the y-axis points upward. Cylindrical coordinates (r,ϕ) are used in the transverse plane, ϕ being the azimuthal angle around the beam pipe. The pseudorapidity is defined in terms of the polar angle θ as $\eta = -\ln\tan(\theta/2)$. For the purpose of the fiducial selection, this is calculated relative to the geometric centre of the detector; otherwise, it is relative to the reconstructed primary vertex of each event.

with scintillator tiles or LAr as active media, and with either steel, copper, or tungsten as the absorber material. The calorimeters cover $|\eta| < 4.9$. The muon spectrometer measures the deflection of muon tracks within $|\eta| < 2.7$ using multiple layers of high-precision tracking chambers located in a toroidal field of approximately 0.5 T and 1 T in the central and end-cap regions of ATLAS, respectively. The muon spectrometer is also instrumented with separate trigger chambers covering $|\eta| < 2.4$.

3 Object Reconstruction

The main physics objects considered in this search are electrons, muons, jets, b jets and missing transverse momentum. A brief summary of the main identification criteria applied for each of these physics objects is given below.

Electron candidates [29] are reconstructed from energy deposits (clusters) in the EM calorimeter that are associated to reconstructed tracks in the inner detector. They are required to have a transverse energy, E_{T}, greater than 25 GeV (where $E_{\mathrm{T}} = E_{\mathrm{cluster}}/\cosh\eta_{\mathrm{track}}$) and $|\eta_{\mathrm{cluster}}| < 2.47$ (where $|\eta_{\mathrm{cluster}}|$ is the pseudorapidity of the cluster associated with the electron candidate). Candidates in the calorimetry transition region $1.37 < |\eta_{\mathrm{cluster}}| < 1.52$ are excluded. The longitudinal impact parameter of the electron track with respect to the selected event primary vertex (see Section 4), z_0, is required to be less than 2 mm. Electrons are required to be separated by $\Delta R > 0.4$ from any selected jet (see below). To reduce the background from non-prompt electrons, i.e. from decays of hadrons (including heavy flavour) produced in jets, electron candidates are required to be isolated. An η-dependent, 90% efficient isolation cut, based on the energy sum of cells around the direction of each candidate, is made for a cone of radius $R = \sqrt{(\Delta\phi)^2 + (\Delta\eta)^2} = 0.2$. This energy sum excludes cells associated with the electron cluster and is corrected for leakage from the electron cluster itself. A further 90% efficient isolation cut is made on the track transverse momentum (p_{T}) sum around the electron in a cone of radius $R = 0.3$.

Muon candidates are reconstructed from track segments in the various layers of the muon spectrometer, and matched with tracks found in the inner detector. The final candidates are refitted using the complete track information from both detector systems, and required to satisfy $p_{\mathrm{T}} > 25$ GeV and $|\eta| < 2.5$. Muons are required to have a hit pattern in the inner detector consistent with a well-reconstructed track. Analogously to the electrons, the muon track longitudinal impact parameter with respect to the primary vertex, z_0, is required to be less than 2 mm. Additionally, muons are required to be separated by $\Delta R > 0.4$ from any selected jet. Muons are required to satisfy a p_{T}-dependent track-based isolation requirement that has good performance even under high pileup conditions or in boosted configurations where the muon is close to a jet: the scalar sum of the track p_{T} in a cone of variable radius $R = 10\ \mathrm{GeV}/p_{\mathrm{T}}^{\mu}$ around the muon (excluding the muon track itself) must be less than 5% of the muon p_{T}.

Jets are reconstructed with the anti-k_t algorithm [30–32] with a radius parameter $R = 0.4$ from calibrated topological clusters [28] built from energy deposits in the calorimeters. Prior to jet finding, a local cluster calibration scheme [33, 34] is applied to correct the topological cluster energies for the effects of non-compensation, dead material and out-of-cluster leakage. The corrections are obtained from simulations of charged and neutral particles. After energy calibration [35], jets are required to have $p_{\mathrm{T}} > 25$ GeV and $|\eta| < 2.5$.

To avoid selecting jets from additional pp interactions in the same bunch crossing, a selection on the so-called "jet vertex fraction" (JVF) variable above 0.5 is applied, representing a requirement that at least 50% of the sum of the p_{T} of tracks with $p_{\mathrm{T}} > 1$ GeV associated with a jet, comes from tracks compatible with originating from the primary vertex.

Jets are identified as originating from the hadronisation of a b quark (b tagging) via an algorithm [36] using multivariate techniques to combine information from the impact parameters of displaced tracks as well as topological properties of secondary and tertiary decay vertices reconstructed within the jet. The working point used for this search corresponds to 70% efficiency to tag a b-quark jet, with a light-

jet rejection factor of ~130 and a charm jet rejection factor of 5, as determined for b-tagged jets with $p_{\mathrm{T}} > 20$ GeV and $|\eta| < 2.5$ in simulated $t\bar{t}$ events.

The missing transverse momentum ($E_{\mathrm{T}}^{\mathrm{miss}}$) is used to estimate the transverse momentum of an assumed neutrino originating from the leptonic decay of one of the W bosons in the $T\bar{T} \to WbWb$ process. $E_{\mathrm{T}}^{\mathrm{miss}}$ is reconstructed by first matching each calorimeter energy cluster with a high-p_{T} object, either a reconstructed lepton or a jet. The energies of cells belonging to these clusters are corrected using the calibration constants associated with the high-p_{T} object. Clusters not associated with a high-p_{T} object are then calibrated for energy losses in un-instrumented regions and for different responses of the calorimeters to electromagnetic and hadronic shower components. This calibration scheme is similar to that described in Ref. [37]. $E_{\mathrm{T}}^{\mathrm{miss}}$ is calculated from a vector sum of the calibrated cluster momenta, together with a term associated with muon momenta.

4 Event Preselection

This search is based on pp collision data at $\sqrt{s} = 8$ TeV collected by the ATLAS experiment between April and October 2012. Only events collected using a single electron or muon trigger under stable beam conditions and for which all detector subsystems were operational are considered. The corresponding integrated luminosity is 14.3 fb^{-1}. Triggers with different p_{T} thresholds are combined in a logical OR in order to maximise the overall efficiency. The p_{T} thresholds are 24 or 60 GeV for electrons and 24 or 36 GeV for muons. The triggers with the lower p_{T} threshold include isolation requirements on the candidate lepton, resulting in inefficiencies at high p_{T} that are recovered by the triggers with higher p_{T} threshold. The triggers use similar but looser selection criteria to the final reconstruction requirements.

Events accepted by the trigger are required to have at least one reconstructed vertex with at least five associated tracks, consistent with the beam collision region in the $x - y$ plane. If more than one vertex is found, the primary vertex is taken to be the one which has the largest sum of the squared transverse momenta of its associated tracks.

Events are required to have exactly one reconstructed electron or muon firing the trigger and at least four jets satisfying the quality and kinematic criteria discussed in Section 3. In addition, at least one b-tagged jet is required. The background from multijet production is suppressed by a requirement on $E_{\mathrm{T}}^{\mathrm{miss}}$ as well as on the transverse mass [3] of the lepton and $E_{\mathrm{T}}^{\mathrm{miss}}$ (m_{T}). For both electron and muon channels the requirements are $E_{\mathrm{T}}^{\mathrm{miss}} > 20$ GeV and $E_{\mathrm{T}}^{\mathrm{miss}} + m_{\mathrm{T}} > 60$ GeV. Finally, events with $\geq$6 jets and $\geq$3 b-tagged jet are rejected, in order to avoid overlap with the events selected by a recent search for $T\bar{T} \to Ht + X$, with $H \to b\bar{b}$ [24].

5 Background and Signal Modelling

After event preselection the main background is $t\bar{t}$+jets production, with the production of a W boson in association with jets (W+jets) and multijet events contributing to a lesser extent. Small contributions arise from single top quark, Z+jets and diboson (WW, WZ, ZZ) production, as well as from the associated production of a vector boson and a $t\bar{t}$ pair. Multijet events contribute to the selected sample via the misidentification of a jet or a photon as an electron or the presence of a non-prompt lepton, e.g. from a semileptonic b- or c-hadron decay, and the corresponding yield is estimated via data-driven methods [38]. For the W+jets background, predictions for the shape of kinematic variables are obtained from the simulation but the normalisation is determined from the data, using the predicted asymmetry between W^++jets and W^-+jets production in pp collisions [39], and separating the events into categories based

[3] $m_{\mathrm{T}} = \sqrt{2p_{\mathrm{T}}^{\ell}E_{\mathrm{T}}^{\mathrm{miss}}(1 - \cos\Delta\phi)}$, where p_{T}^{ℓ} is the transverse momentum (energy) of the muon (electron) and $\Delta\phi$ is the azimuthal angle separation between the lepton and the direction of the missing transverse momentum.

on the multiplicity of b and c jets. Details of the estimation of the multijet and W+jets backgrounds are given in Section 6. The rest of the backgrounds, as well as the signal, are estimated from the simulation and normalised using their theoretical cross sections. In the case of the $t\bar{t}$+jets background prediction, further corrections to match the data are applied, as discussed in Section 7.

Simulated samples of $t\bar{t}$ and single top quark backgrounds (in the s channel and for the associated production with a W boson) are generated with MC@NLO v4.01 [40–42] using the CT10 set of parton distribution functions (PDFs) [43]. In the case of t channel single top quark production, the AcerMC v3.8 leading-order (LO) generator [44] with the MRST LO** PDF set [45] is used. The parton-shower and fragmentation steps are performed by Herwig v6.520 [46] in the case of MC@NLO, and by Pythia 6.421 [47] in the case of AcerMC. These samples are generated assuming a top quark mass of 172.5 GeV and are normalized to approximate next-to-next-to-LO (NNLO) theoretical cross sections [48–51]. The $t\bar{t}$ cross section used is $\sigma_{t\bar{t}} = 238^{+22}_{-24}$ pb, and has been computed with Hathor 1.2 [48] using the MSTW2008 NNLO PDF set [52]. The total uncertainty results from the sum in quadrature of the scale and PDF+α_S uncertainties according to the MSTW prescription [53].

Samples of W/Z+jets events are generated with up to five additional partons using the Alpgen v2.13 [54] LO generator and the CTEQ6L1 PDF set [55], interfaced to Herwig v6.520 for parton showering and fragmentation. To avoid double-counting of partonic configurations in W/Z+jets events generated by both the matrix-element calculation and the parton shower, a parton-jet matching scheme ("MLM matching") [56] is employed. The W+jets samples are generated separately for W+light jets, $Wb\bar{b}$+jets, $Wc\bar{c}$+jets, and Wc+jets, and their relative contributions are normalized using the fraction of b-tagged jets in W+1-jet and W+2-jets data control samples [57]. The Z+jets samples are generated separately for Z+light jets, $Zb\bar{b}$+jets, and $Zc\bar{c}$+jets. The Z+jets background is normalized to the inclusive NNLO theoretical cross section [58]. Overlap between $W/ZQ\bar{Q}$+jets ($Q = b, c$) events generated from the matrix element calculation and those generated from parton-shower evolution in the W/Z+light jets samples is avoided via an algorithm based on the angular separation between the extra heavy quarks. The diboson backgrounds are modeled using Herwig with the MRST LO** PDF set, and are normalized to their NLO theoretical cross sections [59]. Samples of $t\bar{t}V$ ($V = W, Z$) are generated with the Madgraph v5 LO generator [60] and the CTEQ6L1 PDF set and are normalised to the NLO cross section predictions [61, 62]. Parton shower and fragmentation are modelled with Pythia 6.425. Samples of $t\bar{t}H$ are generated with the Pythia 6.425 [47] LO generator and the MRST LO** PDF set [45], assuming a Higgs boson mass of 125 GeV and considering the $H \to b\bar{b}$, $c\bar{c}$, gg, and W^+W^- decay modes. The $t\bar{t}H$ samples are normalised using the NLO theoretical cross section and branching ratio predictions [63]. The $t\bar{t}V$ and $t\bar{t}H$ samples are also generated assuming a top quark mass of 172.5 GeV.

For vector-like T signals, samples corresponding to a singlet T quark decaying to Wb, Zt and Ht are generated with the Protos v2.2 LO generator [10, 64] using the MSTW2008 LO PDF set, and interfaced to Pythia for the parton shower and fragmentation. The predicted branching ratios in the weak-isospin singlet and doublet scenarios as a function of m_T are shown in Fig. 1a. The m_T values considered range from 350 GeV to 850 GeV in steps of 50 GeV, and the Higgs boson mass is assumed to be 125 GeV. All Higgs boson decay modes are considered, with branching ratios as predicted by hdecay [65]. Signal samples are normalized to the approximate NNLO theoretical cross sections [48] using the MSTW2008 NNLO PDF set. The theoretical cross sections as a function of m_T are shown in Fig. 1b.

All event generators using Herwig are also interfaced to Jimmy v4.31 [66] to simulate the underlying event. With the exception of the Protos samples, all simulated samples utilise Photos 2.15 [67] to model photon radiation and Tauola 1.20 [68] to model τ decays. Finally, all simulated samples include multiple pp interactions and are processed through a simulation [69] of the detector geometry and response using Geant4 [70], with the exception of the signal samples, for which a fast simulation of the calorimeter response is used. All simulated samples are processed through the same reconstruction software as the data. Additional corrections are applied so that the object identification efficiencies, energy scales and

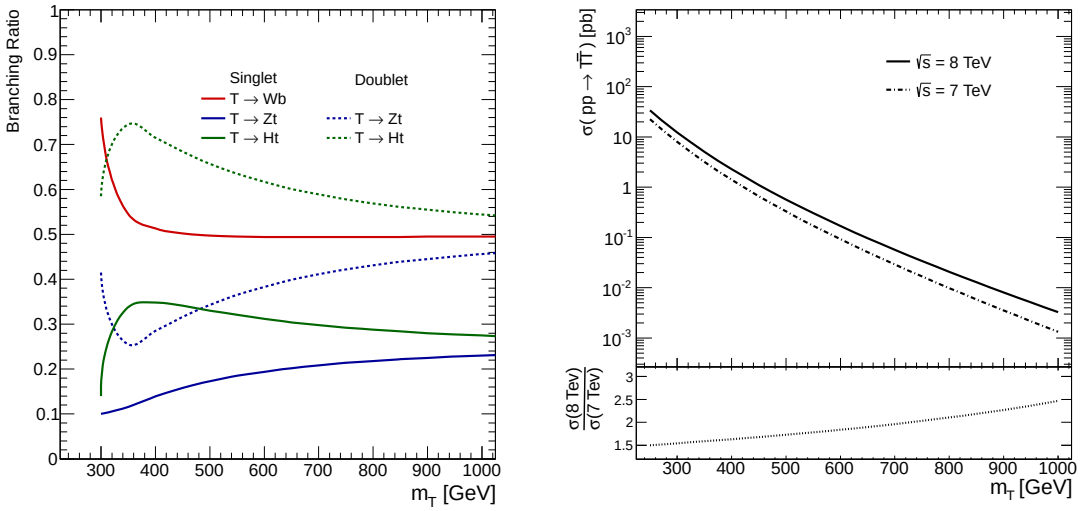

(a) (b)

Figure 1: (a) Branching ratios for T decay as a function of m_T as computed with PROTOS in the weak-isospin singlet and doublet scenarios. (b) Theoretical cross sections at NNLO for $T\bar{T}$ production in pp collisions at two center-of-mass energies, $\sqrt{s} = 7$ TeV and $\sqrt{s} = 8$ TeV, as a function of m_T as computed by HATHOR. Also shown is the ratio of production cross sections between both center-of-mass energies.

energy resolutions match those determined in data control samples.

6 Data-Driven Background Estimates

The multijet and W+jets backgrounds are determined with data. The methods for these determinations are described in the following sections.

6.1 Multijet Background

Multijet events can enter the selected data sample through several production and mis-reconstruction mechanisms. In the electron channel, the multijet background consists of both non-prompt electrons and "fake" electrons, where the latter includes both electrons from photon conversions and mis-identified jets with a high fraction of their energy deposited in the EM calorimeter. In the muon channel, the background contributed by multijet events is predominantly due to non-prompt muons, such as those from semileptonic b- or c-hadron decays.

The multijet background normalisation and shape are estimated directly from data by using the "Matrix Method" (MM) technique [38]. The MM exploits differences in lepton identification-related properties between prompt, isolated leptons from W and Z boson decays (referred to as "real leptons" below) and those where the leptons are either non-isolated or result from the mis-identification of photons or jets. For this purpose, two samples are defined after imposing the final kinematic selection criteria, differing only in the lepton identification criteria: a "tight" sample and a "loose" sample, the former being a subset of the latter. The tight selection employs the final lepton identification criteria used in the analysis. For the loose selection the lepton isolation requirements are omitted. The method assumes that the number of selected events in each sample (N^{loose} and N^{tight}) can be expressed as a linear combination of the numbers of events with real and fake leptons, in such a way that the following system of equations

applies:

$$\begin{aligned} N^{\text{loose}} &= N^{\text{loose}}_{\text{real}} + N^{\text{loose}}_{\text{fake}}, \\ N^{\text{tight}} &= \epsilon_{\text{real}} N^{\text{loose}}_{\text{real}} + \epsilon_{\text{fake}} N^{\text{loose}}_{\text{fake}}, \end{aligned} \tag{1}$$

where ϵ_{real} (ϵ_{fake}) represents the probability for a real (fake) lepton that satisfies the loose criteria to also satisfy the tight ones, and both are measured in data control samples. To measure ϵ_{real} samples enriched in real leptons from W bosons decays are selected by requiring high $E_{\text{T}}^{\text{miss}}$ or m_{T}. The average ϵ_{real} is ~0.75 (~0.98) in the electron (muon) channel. To measure ϵ_{fake} samples enriched in multijet background are selected by requiring either low $E_{\text{T}}^{\text{miss}}$ (electron channel) or high impact parameter significance for the lepton track (muon channel). The average ϵ_{fake} value is ~0.35 (~0.20) in the electron (muon) channel. Dependences of ϵ_{real} and ϵ_{fake} on quantities such as lepton p_{T} and η, ΔR between the lepton and the closest jet, or number of b-tagged jets, are taken into account in order to obtain a more accurate estimate.

6.2 W+jets Background

The estimate of the W+jets background is based on data for its normalisation and on the simulation for its shape. In proton-proton collisions W+jets production is charge asymmetric. The total number of W+jets events in data, $N_W = N_{W^+} + N_{W^-}$, can be estimated based on the measured difference between the number of positively- and negatively-charged W bosons, $(N_{W^+} - N_{W^-})_{\text{meas}}$, and the asymmetry predicted from the simulation:

$$N_W = \left(\frac{N_{W^+} + N_{W^-}}{N_{W^+} - N_{W^-}} \right)_{\text{MC}} (N_{W^+} - N_{W^-})_{\text{meas}} \, . \tag{2}$$

The simulation overestimates the number of W+jets events compared to the data-driven determination by up to ~20%, depending on the jet multiplicity. Corresponding scale factors to correct the prediction from the simulation have been derived [71] using Eq. (2) separately for W+4 jets and W+≥5 jets events and are used in this analysis to calibrate the W+jets background to data before b tagging. Scale factors for the fractions of $Wb\bar{b}$+jets, $Wc\bar{c}$+jets and Wc+jets are also determined from data [71] and are used to correct the simulation. These factors are determined by simultaneously analysing W+2 jets events with 0 b tagged jets and with ≥1 b-tagged jets. The fraction of W+light jets events is scaled accordingly in order to preserve the overall normalisation of the W+jets background before b tagging.

7 Final Event Selection

After preselection, further background suppression is achieved by applying requirements aimed at exploiting the distinct kinematic features of the signal. The large T quark mass results in energetic W bosons and b quarks in the final state with large angular separation between them, while the decay products from the boosted W bosons have small angular separation. The combination of these properties is very effective in suppressing the dominant $t\bar{t}$ background since $t\bar{t}$ events with boosted W boson configurations are rare, and are typically characterized by a small angular separation between the W boson and b quark from the top quark decay.

To take advantage of these properties, it is necessary to identify the hadronically-decaying W boson (W_{had}) as well as the b jets in the event. The candidate b jets are defined as the two jets with the highest b-tag discriminant (although only one of them is explicitly required to be b tagged in the event selection). Two types of W_{had} candidates are defined, $W_{\text{had}}^{\text{type I}}$ and $W_{\text{had}}^{\text{type II}}$, depending on the angular separation between their decay products. $W_{\text{had}}^{\text{type I}}$ candidates correspond to boosted W bosons, where the quarks from the W boson decay have small angular separation between them and are reconstructed as a single jet. $W_{\text{had}}^{\text{type II}}$ candidates correspond to W bosons where both quarks from the W boson decay are

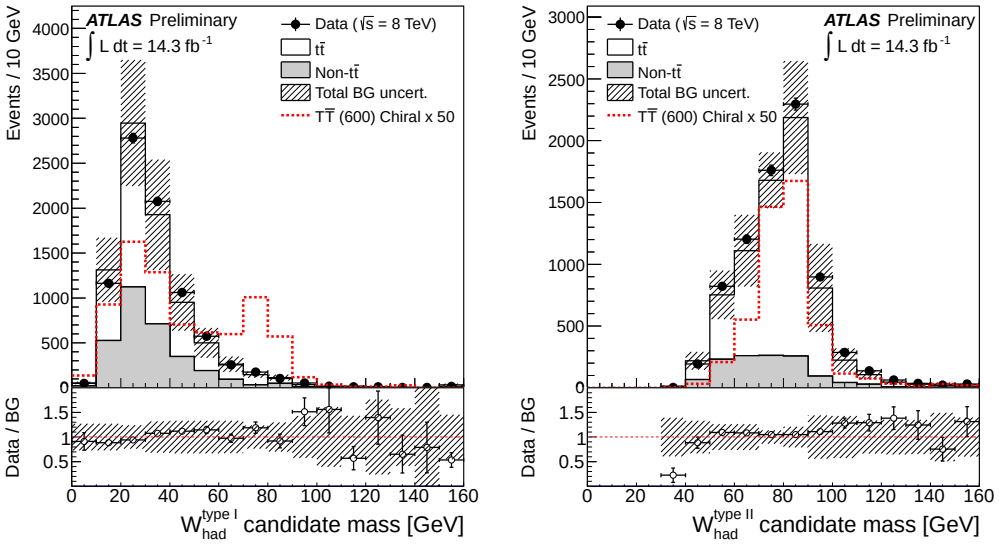

(a) (b)

Figure 2: Distribution of the reconstructed mass for (a) $W_{\text{had}}^{\text{type I}}$ and (b) $W_{\text{had}}^{\text{type II}}$ candidates for the combined e+jets and μ+jets channels after preselection. These events have ≥ 1 W_{had} candidates (see text for details) but have not had the mass requirement imposed. The data (solid black points) are compared to the SM prediction (stacked histograms). The total uncertainty on the background estimation (see Section 9 for details) is shown as a black hashed band. The expected contribution from a chiral fourth-generation T quark with mass $m_T = 600$ GeV, multiplied by a factor of 50, is also shown (red dashed histogram). The lower panel shows the ratio of data to SM prediction. The overflow has been added to the last bin.

reconstructed as separate jets. In the construction of both types of W_{had} candidates, the two candidate b jets are excluded from consideration. $W_{\text{had}}^{\text{type I}}$ is defined as a single jet with $p_{\text{T}} > 250$ GeV and mass in the range of 60–120 GeV. The asymmetric window about the world-average W boson mass value is chosen in order to increase the acceptance for hadronically-decaying Z bosons. The mass distribution for $W_{\text{had}}^{\text{type I}}$ candidates, prior to the jet mass requirement itself, is shown in Fig. 2. $W_{\text{had}}^{\text{type II}}$ is defined as a dijet system with $p_{\text{T}} > 200$ GeV, angular separation $\Delta R(j, j) < 0.8$ and mass within the range of 60–120 GeV. Any jets satisfying the $W_{\text{had}}^{\text{type I}}$ requirements are excluded from consideration to form $W_{\text{had}}^{\text{type II}}$ candidates. If multiple pairs satisfy the above requirements, the one with mass closest to the nominal W boson mass is chosen. The mass distribution for $W_{\text{had}}^{\text{type II}}$ candidates, prior to the dijet mass requirement, is shown in Fig. 2. Figure 3a shows the number of W_{had} candidates after preselection.

The leptonically-decaying W boson is reconstructed using the lepton and $E_{\text{T}}^{\text{miss}}$, which is identified as the neutrino p_{T}. Requiring that the invariant mass of the lepton–neutrino system equals the nominal W boson mass allows reconstruction of the neutrino longitudinal momentum up to a two-fold ambiguity. If two solutions exist, they are both considered (see Section 8). If no real solution exists, the neutrino pseudorapidity is set equal to that of the lepton, since in the kinematic regime of interest the decay products of the W boson tend to be collinear.

Two final selections, *loose* and *tight*, are defined (see Table 1 for a summary). The *loose* selection considers events with ≥ 4 jets and with at least one $W_{\text{had}}^{\text{type I}}$ or $W_{\text{had}}^{\text{type II}}$ candidate. The events must satisfy $H_{\text{T}} > 800$ GeV, where H_{T} is the scalar sum of the lepton p_{T}, $E_{\text{T}}^{\text{miss}}$ and the p_{T} of the four highest-p_{T} jets. The H_{T} distribution peaks at $\sim 2m_T$ for signal events, which makes the $H_{\text{T}} > 800$ GeV requirement particularly efficient for signal with $m_T \gtrsim 400$ GeV, while rejecting a large fraction of the background. Figure 3b shows the distribution of H_{T} prior to the $H_{\text{T}} > 800$ GeV requirement. In

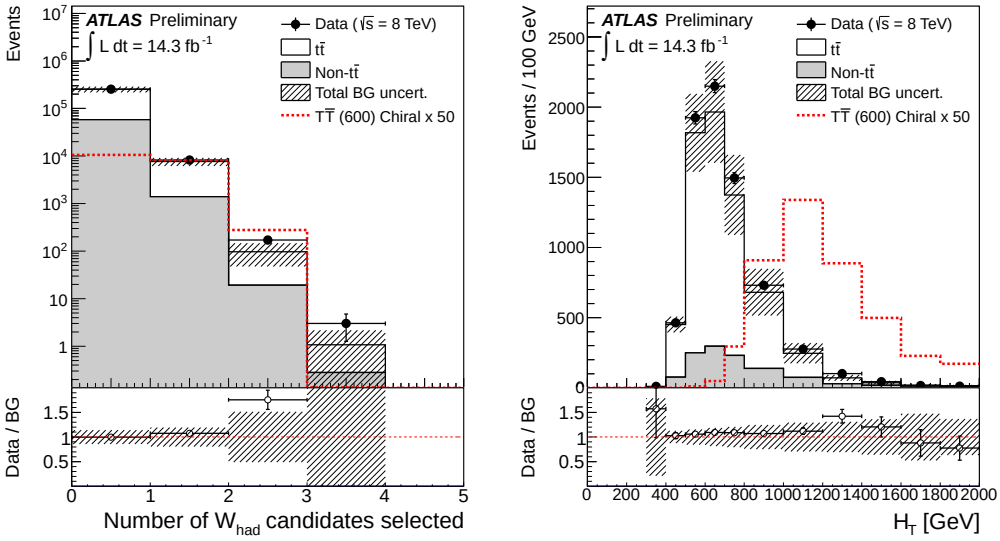

(a) (b)

Figure 3: Distribution of (a) number of W_{had} candidates at the preselection level, and (b) H_{T} after requirement of ≥ 1 W_{had} candidate, for the combined e+jets and μ+jets channels. The data (solid black points) are compared to the SM prediction (stacked histograms). The total uncertainty on the background estimation (see Section 9 for details) is shown as a black hashed band. The expected contribution from a chiral fourth-generation T quark with mass $m_T = 600$ GeV, multiplied by a factor of 50, is also shown (red dashed histogram), The lower panel shows the ratio of data to SM prediction. The overflow has been added to the last bin.

Table 1: Summary of event selection requirements.

Selection	Requirements
Preselection	One electron or muon
	$E_{\text{T}}^{\text{miss}} > 20$ GeV, $E_{\text{T}}^{\text{miss}} + m_{\text{T}} > 60$ GeV
	≥ 4 jets, ≥ 1 b-tagged jets
loose selection	Preselection
	≥ 1 W_{had} candidates
	$H_{\text{T}} > 800$ GeV
	$p_{\text{T}}(b_1) > 160$ GeV, $p_{\text{T}}(b_2) > 80$ GeV
	$\Delta R(\ell, \nu) < 1.2$
tight selection	*loose* selection
	$\min\Delta R(\ell, b) > 1.4$, $\min\Delta R(W_{\text{had}}, b) > 1.4$

addition, the highest-p_{T} b-jet candidate (b_1) and the next-to-highest-p_{T} b-jet candidate (b_2) are required to have $p_{\text{T}} > 160$ GeV and $p_{\text{T}} > 80$ GeV, respectively. Figure 4 shows the distributions of $p_{\text{T}}(b_1)$ and $p_{\text{T}}(b_2)$ after all previous requirements and prior to the $p_{\text{T}}(b_1)$ and $p_{\text{T}}(b_2)$ requirements, respectively. Finally, the angular separation between the lepton and the reconstructed neutrino is required to satisfy $\Delta R(\ell, \nu) < 1.2$. The *tight* selection adds the following isolation requirements to the *loose* selection: $\min(\Delta R(W_{\text{had}}, b_{1,2})) > 1.4$ and $\min(\Delta R(\ell, b_{1,2})) > 1.4$, which are particularly effective at suppressing $t\bar{t}$ background. If an event has multiple W_{had} candidates, the one with highest p_{T} is selected. Figure 5

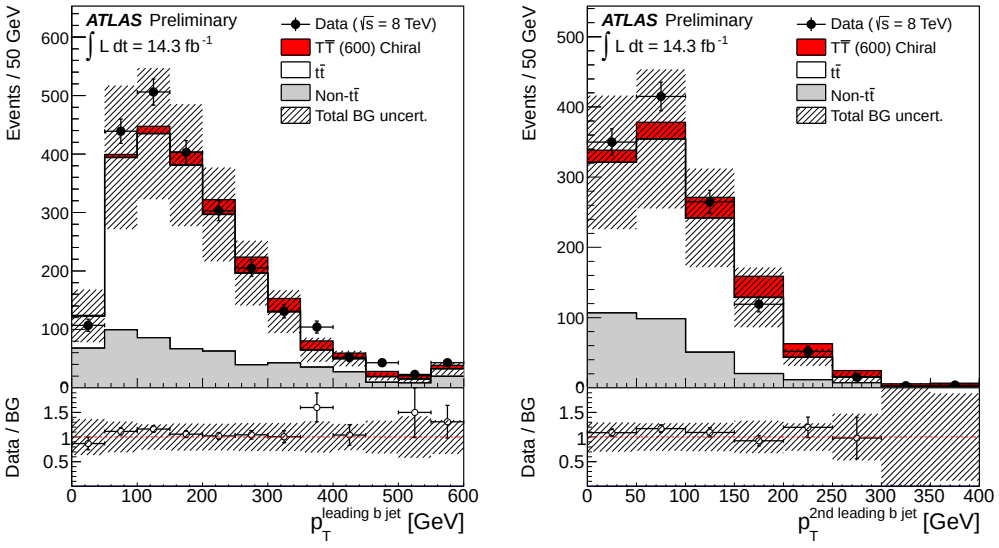

(a) (b)

Figure 4: Distribution of (a) p_{T} of leading b jet candidate, $p_{\mathrm{T}}(b_1)$, and (b) p_{T} of subleading b jet candidate, $p_{\mathrm{T}}(b_2)$, for the combined e+jets and μ+jets channels after all previous selection requirements (see text for details), except for the requirements on $p_{\mathrm{T}}(b_1)$ and $p_{\mathrm{T}}(b_2)$ themselves. The data (solid black points) are compared to the SM prediction (stacked histograms). The total uncertainty on the background estimation (see Section 9 for details) is shown as a black hashed band. The expected contribution from a chiral fourth-generation T quark with mass $m_T = 600$ GeV is also shown (red shaded histogram), stacked on top of the SM background. The lower panel shows the ratio of data to SM prediction. The overflow has been added to the last bin.

shows the distributions of $\Delta R(\ell, \nu)$ and $\min(\Delta R(\ell, b_{1,2}))$ after all previous requirements and prior to the $\Delta R(\ell, \nu)$ and $\min(\Delta R(\ell, b_{1,2}))$ requirements, respectively.

Table 2 presents a summary of the background estimates for the *loose* and *tight* selections, respectively, as well as a comparison of the total predicted and observed yields. The quoted uncertainties include both statistical and systematic contributions. The latter are discussed in Section 9. The predicted and observed yields are in agreement within these uncertainties.

8 Heavy Quark Mass Reconstruction

The main discriminant variable used in this search is the reconstructed heavy-quark mass (m_{reco}), built from the W_{had} candidate and one of the two b-jet candidates. The reconstruction of the leptonically-decaying W boson usually yields two solutions, and there are two possible ways to pair the b-jet candidates with the W boson candidates to form the heavy quarks. Among all possible combinations, the one yielding the smallest absolute difference between the two reconstructed heavy quark masses is chosen. The resulting m_{reco} distributions in Fig. 6 show that the SM background has been effectively suppressed, and that, as is most visible for the *loose* selection, good discrimination between signal and background is achieved. The small contributions from W+jets, Z+jets, diboson, single-top and multi-jet events are combined into a single background source referred to as non-$t\bar{t}$. It was verified *a priori* that the *tight* selection has the better sensitivity, and it is therefore chosen to derive the final result for the search. The *loose* selection, displaying a significant $t\bar{t}$ background at low m_{reco} which is in good agreement with the expectation, provides further confidence in the background modeling prior to the application of b-jet

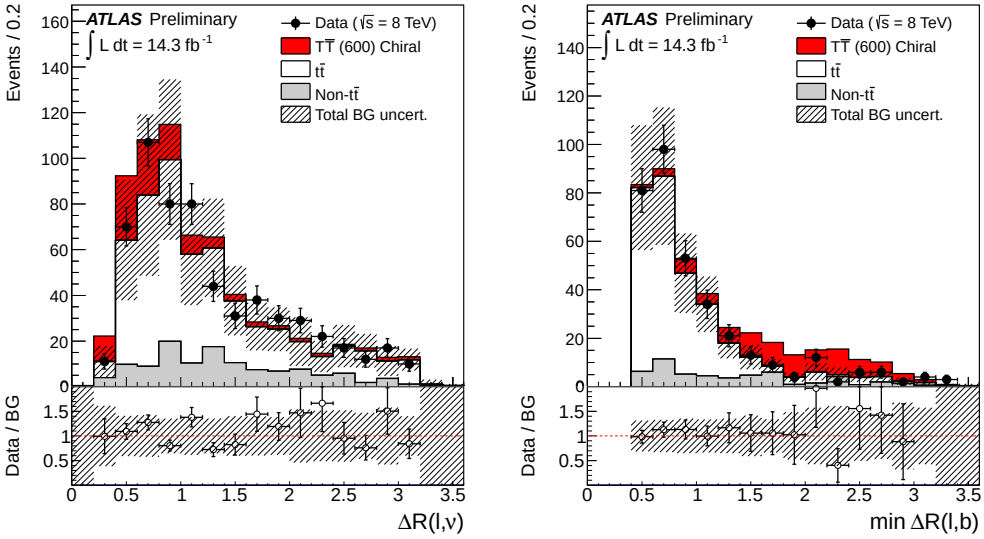

(a) (b)

Figure 5: Distribution of (a) $\Delta R(\ell, \nu)$ and (b) $\min(\Delta R(\ell, b_{1,2})) > 1.4$ for the combined e+jets and μ+jets channels after all previous selection requirements (see text for details), except for the requirements on $\Delta R(\ell, \nu)$ and $\min(\Delta R(\ell, b_{1,2})) > 1.4$ themselves. In the case of (b), this corresponds to the *loose* selection. The data (solid black points) are compared to the SM prediction (stacked histograms). The total uncertainty on the background estimation (see Section 9 for details) is shown as a black hashed band. The expected contribution from a chiral fourth-generation T quark with mass $m_T = 600$ GeV is also shown (red shaded histogram), stacked on top of the SM background. The lower panel shows the ratio of data to SM prediction. The overflow has been added to the last bin.

Table 2: Number of observed events, integrated over the whole mass spectrum, compared to the SM expectation for the combined e+jets and μ+jets channels after the *loose* and *tight* selections. The expected signal yields in two different scenarios, a chiral fourth-generation T quark and a vector-like singlet T quark, assuming $m_T = 600$ GeV, are also shown. The quoted uncertainties include both statistical and systematic contributions.

	loose selection	*tight* selection
$t\bar{t}$	264 ± 80	10 ± 6
$t\bar{t}V$	5.1 ± 1.8	0.5 ± 0.2
W+jets	16 ± 11	6 ± 5
Z+jets	1.1 ± 1.4	0.2 ± 0.5
Single top	30 ± 7	4.4 ± 1.6
Dibosons	0.21 ± 0.15	0.06 ± 0.05
Total background	317 ± 90	21 ± 9
Data	348	37
$T\bar{T}(600$ GeV)		
Chiral fourth-generation	88 ± 10	54 ± 7
Vector-like singlet	41 ± 4	20.3 ± 2.2

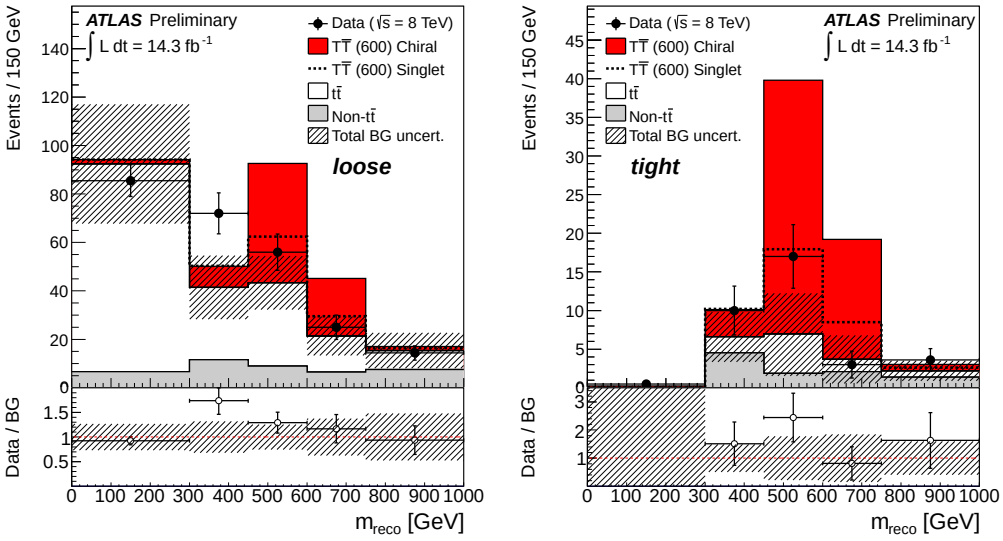

(a) (b)

Figure 6: Distribution of m_{reco} for the combined e+jets and μ+jets channels after the (a) *loose* and (b) *tight* selection. The data (solid black points) are compared to the SM prediction. The shaded area represents the total background uncertainty (see Section 9 for details). Also shown, stacked on top of the SM background, is the expected contribution from signal corresponding to a chiral T quark with mass $m_T = 600$ GeV. The overflow has been added to the last bin.

isolation requirements in the *tight* selection.

9 Systematic Uncertainties

Several sources of systematic uncertainties have been considered that can affect the normalisation of signal and background and/or the shape of their corresponding final discriminant distributions. Individual sources of systematic uncertainty are considered uncorrelated. Correlations of a given systematic uncertainty are maintained across processes. Table 3 presents a summary of the systematic uncertainties considered in the analysis indicating whether they are taken to be normalisation-only, or to affect both shape and normalisation. The following sections describe each of the systematic uncertainties considered in the analysis.

9.1 Luminosity

The luminosity estimate has an uncertainty of 3.6% [72]. This systematic uncertainty is applied to all processes except the multijet background.

9.2 Uncertainties on Object Definitions

In this section uncertainties in the reconstruction of jets, leptons and b-, c-, and light flavour-tagging are considered.

Table 3: List of all systematic uncertainties (in %) considered in the analysis, indicating which ones are treated as normalisation and/or shape uncertainties, with their impact on normalisation in the case of the *tight* selection, for signal and backgrounds. The signal given here is a chiral fourth-generation T quark with mass $m_T = 600$ GeV.

	$T\bar{T}$ (600 GeV)	$t\bar{t}$	Non-$t\bar{t}$
Uncertainties [%] affecting only the normalisation of the m_{reco} distribution:			
Luminosity	+3.6/-3.6	+3.6/-3.6	+3.6/-3.6
Lepton trigger, reconstruction and ID efficiency	+2.0/-2.0	+2.0/-2.0	+2.0/-2.0
$t\bar{t}$ cross section	–	+10/-11	–
Uncertainties [%] affecting both normalisation and shape of the m_{reco} distribution:			
Jet energy scale	+6.6/-8.4	+15/-15	+33/-22
Jet energy resolution	+8.4/-8.4	+3.6/-3.6	+9.3/-9.3
Jet identification efficiency	+2.3/-2.7	+2.3/-2.5	+1.9/-2.6
b-quark tagging efficiency	+6.7/-7.3	+6.7/-8.9	+1.8/-2.2
c-quark tagging efficiency	+1.6/-1.6	+4.1/-4.1	+5.6/-5.6
Light-jet tagging efficiency	+0.3/-0.3	+0.7/-0.7	+2.7/-2.7
$t\bar{t}$ modelling: NLO MC generator	–	+48/-48	–
$t\bar{t}$ modelling: parton shower and fragmentation	–	+25/-25	–
$t\bar{t}$ modelling: initial and final state QCD radiation	–	+8.8/-8.8	–
W+jets normalisation	–	–	+8.9/-7.8
W+heavy-flavor fractions	–	–	+18/-19
W+jets modelling: scale variation	–	–	+11/-11
Z+jets cross section	–	–	+1.1/-1.1
Single top cross section	–	–	+1.9/-1.5
Diboson cross section	–	–	< 0.1%
$t\bar{t}V$ cross section	–	–	+1.5/-1.5
Total	+14/-15	+59/-59	+42/-35

9.2.1 Lepton Reconstruction, Identification and Trigger

The reconstruction and identification efficiency of electrons and muons, as well as the efficiency of the trigger used to record the events, differ between data and simulation. Scale factors are derived using tag-and-probe techniques on $Z \to \ell^+\ell^-$ ($\ell = e, \mu$) data and simulated samples to correct the simulation for these discrepancies. For each source of uncertainty, the quadratic sum of the statistical and systematic uncertainties on the corresponding scale factor is taken as the overall systematic uncertainty. A total uncertainty on the signal and background acceptances of 2% is estimated.

9.2.2 Lepton Momentum Scale and Resolution

The accuracy of lepton momentum scale and resolution in simulation is checked using reconstructed distributions of the $Z \to \ell^+\ell^-$ and $J/\psi \to \ell^+\ell^-$ masses. In the case of electrons, E/p studies using $W \to e\nu$ events are also used. Small discrepancies are observed between data and simulation, and corrections for the lepton energy scale and resolution in the latter are applied. In the case of electrons, energy scale corrections need to be applied to data (all regions) and simulation (calorimeter transition region), while energy resolution corrections are applied to the simulation only. In the case of muons, momentum scale and resolution corrections are only applied to the simulation. Uncertainties on both the momentum scale and resolution are considered, and varied separately. The resulting uncertainties

on the total yields predicted by the simulation are at the sub-percent level and therefore neglected in the analysis.

9.2.3 Jet Vertex Fraction Efficiency

The per-jet efficiency to satisfy the |JVF| > 0.5 requirement is measured in $Z(\rightarrow \ell^+\ell^-)$+1-jet events in data and simulation, selecting separately events enriched in hard-scatter jets and events enriched in jets from other proton interactions in the same bunch crossing (pileup). Dedicated data/simulation efficiency and inefficiency scale factors are measured separately for both types of jets. The efficiency scale factor for hard-scatter jets decreases from ∼1.03 at $p_{\mathrm{T}} = 25$ GeV to ∼1.01 for $p_{\mathrm{T}} > 150$ GeV. The scale factors for pileup jets are found to be consistent with 1. The product of all per-jet scale factors define a per-event weight used to calibrate the simulation to data. The propagation of the per-jet scale factor uncertainty results in an overall uncertainty on the signal and background acceptance of ∼2.5%.

9.2.4 Jet Energy Scale

The jet energy scale and its uncertainty have been derived combining information from test-beam data, LHC collision data and simulation [35, 73, 74]. The overall jet energy scale uncertainty in the central detector region ranges from ∼4% at $p_{\mathrm{T}} = 25$ GeV to ∼1% at $p_{\mathrm{T}} = 500$ GeV [75]. The effect of the jet energy scale uncertainty is assessed by varying the jet p_{T} of all selected jets in the simulation by ±1 standard deviation. The missing transverse momentum is corrected according to the varied p_{T} of the jets in each event and all jet-related kinematic variables are recomputed accordingly.

9.2.5 Jet Energy Resolution

The jet energy resolution has been measured as a function of the jet p_{T} and rapidity using two *in-situ* techniques [35], and found to be consistent between data and simulation. The quadratic difference between the jet energy resolutions for jets in data and the simulation is used to derive a systematic uncertainty in the analysis. The energy of jets in the simulation is smeared by this residual difference, and the changes in the normalisation and shape of the final discriminant is compared to the default (unsmeared) prediction by the simulation. This uncertainty is then symmetrised.

9.2.6 Heavy- and Light-Flavour Tagging

The effects of uncertainties in efficiencies for the heavy flavour identification of jets by the *b*-tagging algorithm have been evaluated. These efficiencies are measured from data and depend on the jet flavour.

Efficiencies for *b* and *c* quarks in the simulation have to be corrected by p_{T}-dependent factors of 0.9–1.0 and 1.1–1.2, respectively, whereas the light jet efficiency has to be scaled up by a factor of ∼1.3. These scale factors have an uncertainty between 7% and 13% for *b* jets, between 15% and 39% for *c* jets, and ∼25% for light jets. The scale factors and their uncertainties are applied to each jet in the simulation depending on its flavour, p_{T} and η [76–78].

A total of nine and five independent sources of uncertainty are considered for the *b*-tagging and *c*-tagging efficiencies, respectively. Each of these uncertainties correspond to a resulting eigenvector after diagonalising the matrix containing the information of total uncertainty per p_{T} bin and the bin-to-bin correlations. These systematic uncertainties are taken as uncorrelated between *b*, *c* jets, and light flavour jets. A per-jet weighting procedure is applied to simulated events to propagate the calibration of *b* tagging and the related uncertainties.

9.3 Normalisations of Data-Driven Backgrounds

In this section the uncertainties in rates of data-driven background estimates are described.

9.3.1 W/Z+jets Normalisation

The W/Z+jets cross sections from ALPGEN are affected by large uncertainties because they are a leading-order calculation. As discussed in Section 6.2, the overall W+jets normalisation is obtained via data-driven methods separately for events with exactly 4 jets and ≥ 5 jets in order to ensure the best possible central value for the predicted W+jets yield. Additional uncertainties are considered on the fractions of $Wb\bar{b}$, $Wc\bar{c}$ and Wc, as well as the their extrapolation from 2-jet events, where they are measured in data, to higher jet multiplicity. The sum in quadrature of the above contributions result in a total uncertainty of ~30% on the estimated W+jets normalisation for events satisfying the *tight* selection.

9.4 Uncertainties on Background Modelling

The following sections describe uncertainties in the rates and shapes of the discriminants arising from estimates based on theoretical calculations.

9.4.1 Theoretical Cross-sections

Uncertainties of +10%/-11% are assumed for the inclusive $t\bar{t}$ production cross section evaluated at approximate NNLO using HATHOR [48]. Uncertainties of +5%/-4% and ±5% are assumed for the theoretical cross sections of the single top [49–51] and diboson [59] backgrounds, respectively. Finally, and uncertainty of ±30% is assumed for the theoretical cross section of the $t\bar{t}V$ [61, 62] background.

9.4.2 $t\bar{t}$ Modelling

A number of systematic uncertainties affecting the modelling of $t\bar{t}$ are considered in this analysis: (1) the choice of NLO event generator, (2) the modeling of initial and final state QCD radiation, and (3) the choice of parton-shower and fragmentation models.

NLO Event Generator: The effect of uncertainties on the parton-level modeling of $t\bar{t}$ is obtained by comparing the distributions from two NLO MCs, MC@NLO and POWHEG, both interfaced to HERWIG. This choice is based on detailed comparisons between data and MC in a number of control regions, often defined starting from the *loose* selection but with one of the cuts inverted to reject a possible signal contribution. In these studies three different $t\bar{t}$ generators, MC@NLO, POWHEG and ALPGEN were compared. In general, it was found that data was bracketed by MC@NLO and POWHEG predictions, with MC@NLO providing the best description overall, which motivated its choice as the main $t\bar{t}$ generator for this analysis. In contrast, ALPGEN was found to be the most inconsistent model with data, predicting yields above POWHEG, which motivated its rejection as a valid alternate $t\bar{t}$ model in the kinematic region explored by this analysis.

Differences between MC@NLO and POWHEG arise from the details on how the NLO calculation is interfaced with the parton shower, resulting in POWHEG predicting higher jet multiplicities than MC@NLO. These two samples have been processed through a fast simulation. The relative uncertainty between POWHEG+HERWIG and MC@NLO fast-simulation samples is symmetrised and propagated to the MC@NLO fully simulated sample. The resulting uncertainty on the $t\bar{t}$ yield after the *tight* selection is 48%, and constitutes the main source of uncertainty on the $t\bar{t}$ background. The corresponding uncertainty after the *loose* selection is 16%. The significant increase in the uncertainty for the *tight* selection primarily results from the increased jet multiplicity in POWHEG compared to MC@NLO, which leads to a larger rate of

misreconstruction of the W_{had} candidate, and renders the $\min(\Delta R(W_{\text{had}}, b_{1,2})) > 1.4$ cut less effective than in the case of MC@NLO.

Initial- and Final-State QCD Radiation: To assess the systematic uncertainty on the modeling of initial-state (ISR) and final-state radiation (FSR), dedicated $t\bar{t}$ samples are generated with AcerMC+Pythia with modified Pythia parameters in order to increase or reduce the amount of parton shower. The range of variation for these parameters is chosen to be consistent with existing measurements such as the gap fraction in dileptonic $t\bar{t}$ events [79] and jet shapes in QCD multijet events. These samples have been processed through a fast simulation. Half the difference between these alternate samples is symmetrised and propagated to the MC@NLO fully-simulated sample, resulting in an uncertainty on the $t\bar{t}$ yield after the *tight* selection of 8.8%.

Parton-Shower and Fragmentation Models: Uncertainties on the simulation of the parton shower and fragmentation are studied comparing two different hadronisation models applied to the same parton level generator: PowHeg+Herwig vs PowHeg+Pythia. These two samples have been processed through a fast simulation. The relative uncertainty between PowHeg+Herwig and PowHeg+Pythia fast-simulation samples is symmetrised and propagated to the MC@NLO fully simulated sample, resulting in an uncertainty on the $t\bar{t}$ yield after the *tight* selection of 25%.

9.4.3 V+jets Modelling

The effect of uncertainties in the modeling of V+jets kinematics by Alpgen is assessed by changing the factorization scale from the nominal choice, $Q^2 = m_{\text{W}}^2 + \sum m_{\text{T}}^2$, to $Q^2 = m_{\text{W}}^2 + p_{\text{T,W}}^2$. This uncertainty is then symmetrised.

10 Statistical Analysis

In the absence of any significant data excess, the m_{reco} spectrum for the *tight* selection shown in Fig. 6 is used to derive 95% CL upper limits on the $T\bar{T}$ production cross section times branching fraction using the CL_{s} method [80, 81]. This method employs a log-likelihood ratio $LLR = -2\log(L_{\text{s+b}}/L_{\text{b}})$ as test-statistic, where $L_{\text{s+b}}$ (L_{b}) is a binned likelihood function, defined as a product of Poisson probabilities per bin, to observe the data under the signal-plus-background (background-only) hypothesis. Pseudo-experiments are generated for both hypotheses, taking into account per-bin statistical fluctuations of the total predictions according to Poisson statistics, as well as Gaussian fluctuations describing the effect of systematic uncertainties. To compute each of the likelihoods, the nuisance parameters describing the effect of systematic uncertainties are taken at their nominal values, i.e. no fitting of nuisance parameters is performed. Therefore, no additional constraints on the magnitude of systematic uncertainties are placed by the data during the statistical analysis. The fraction of pseudo-experiments for the signal-plus-background (background-only) hypothesis with LLR larger than a given threshold defines $CL_{\text{s+b}}$ (CL_{b}). Such a threshold is set to the observed (median) LLR for the observed (expected) limit. Signal cross sections for which $CL_{\text{s}} = CL_{\text{s+b}}/CL_{\text{b}} < 0.05$ are deemed to be excluded at 95% CL. Using CL_{s} instead of $CL_{\text{s+b}}$ minimizes the possibility of mistakenly excluding a small signal due to a downward fluctuation of the background, as this would lead to small values of both $CL_{\text{s+b}}$ and CL_{b}.

11 Results

The consistency of the data with the background prediction is assessed by computing the p-value under the background-only hypothesis, taken to be 1-CL_{b}, for each signal scenario and m_T value considered.

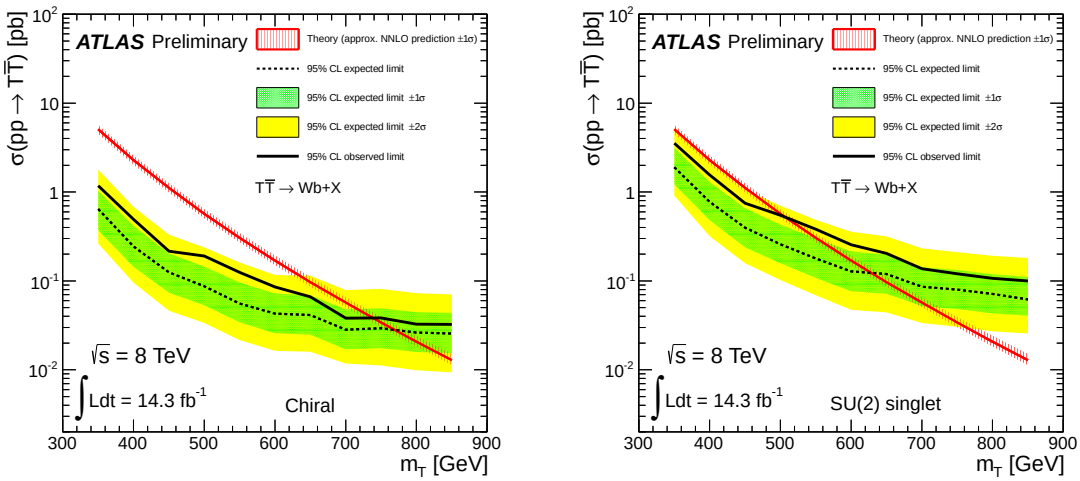

(a) (b)

Figure 7: Observed (solid line) and expected (dashed line) 95% CL upper limits on the $T\bar{T}$ cross section times branching fraction for (a) a chiral fourth-generation T quark and (b) a vector-like singlet T quark as a function of the T quark mass. The surrounding shaded bands correspond to the ±1 and ±2 standard deviations around the expected limit. The thin red line and band show the theoretical prediction and its ±1 standard deviation uncertainty.

The smallest p-value found, 0.095, is obtained for $m_T = 350$ GeV, $BR(T \to Zt) = 0.9$ and $BR(T \to Wb) = BR(T \to Ht) = 0.05$, and corresponds to a significance of 1.7 standard deviations above the background-only prediction, which is not significant.

The resulting observed and expected upper limits on the $T\bar{T}$ production cross section times branching fraction are shown in Fig. 7 as a function of m_T, and compared to the theoretical prediction for two benchmark scenarios: a chiral fourth-generation T quark and a vector-like singlet T quark. The total uncertainty on the theoretical cross section [48] includes the contributions from scale variations and PDF uncertainties. For a chiral fourth-generation T quark, an observed (expected) 95% CL limit $m_T > 740\,(770)$ GeV is obtained for the central value of the theoretical cross section. This represents the most stringent limit to date, and is also applicable to a Y vector-like quark with electric charge of $-4/3$ and decaying into a W^- boson and a b quark. For a vector-like singlet T quark, the observed (expected) 95% CL limit is $m_T > 505\,(630)$ GeV, also for the central value of the theoretical cross section. Systematic uncertainties result in a degradation of the expected cross section limit by ~50% at the highest m_T values explored.

The same analysis is used to derive exclusion limits on vector-like T quark production, for different values of m_T and as a function of the two branching ratios $BR(T \to Wb)$ and $BR(T \to Ht)$. To probe this two-dimensional branching-ratio plane, the signal samples are reweighted by the ratio of desired branching ratio to the original branching ratio in Protos, and the complete analysis is repeated. The resulting 95% CL exclusion limits are shown in Fig. 8 for different values of m_T. For instance, for a T quark with a mass of 600 GeV an observed (expected) 95% CL lower limit of $BR(T \to Wb) < 0.7\,(0.45)$ is obtained, regardless of the value of its branching ratios to Ht and Zt. All the decay modes contribute to the final sensitivity when setting limits. For example, assuming $m_{t'} = 600$ GeV, the acceptance times efficiency of the *tight* selection is 2.45%, 0.64%, 0.47%, 0.10%, 0.18% and 0.16%, for decays to $WbWb$, $WbZt$, $WbHt$, $ZtZt$, $ZtHt$ and $HtHt$, respectively.

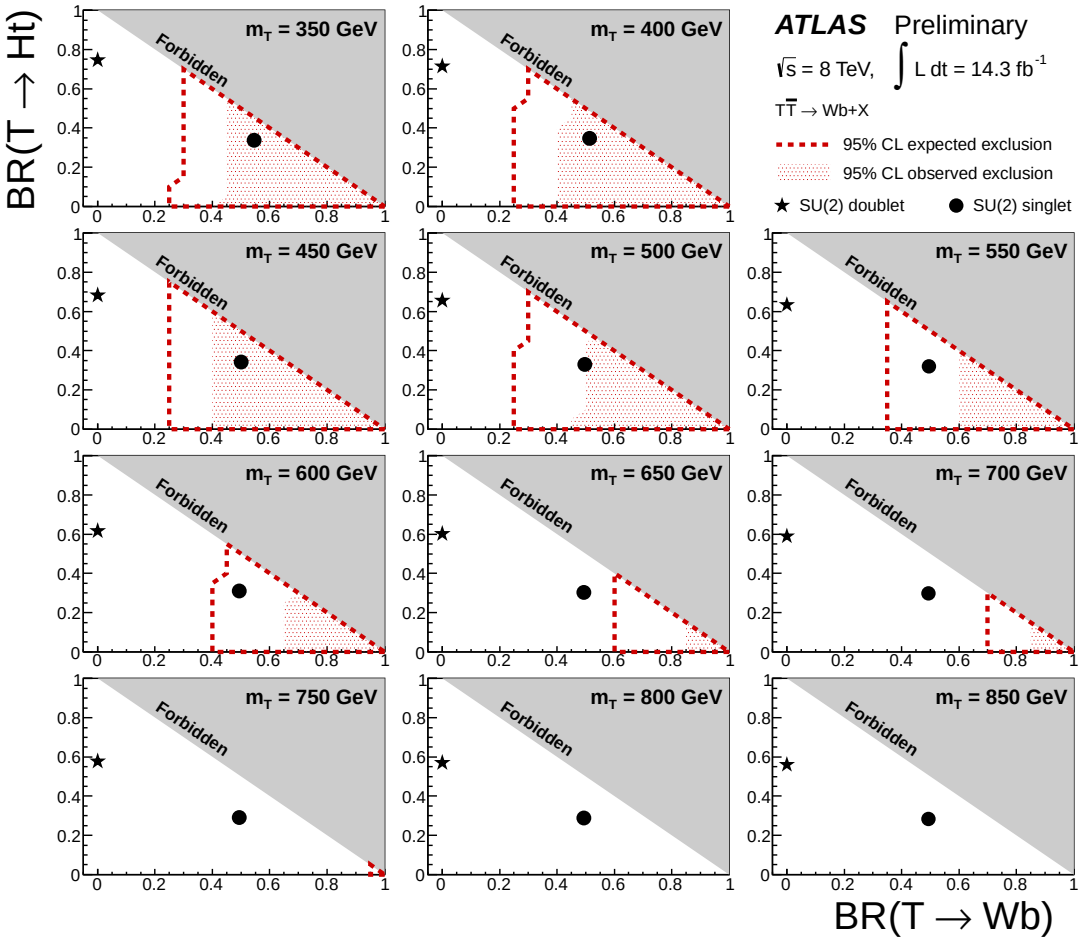

Figure 8: Observed (red filled area) and expected (red dashed line) 95% CL exclusion in the plane of $BR(T \to Wb)$ versus $BR(T \to Ht)$, for different values of the vector-like T quark mass. The grey (dark shaded) area corresponds to the unphysical region where the sum of branching ratios exceeds unity. The default branching ratio values from the Protos event generator for the weak-isospin singlet and doublet cases are shown as plain circle and star symbols, respectively. This result includes both statistical and systematic uncertainties.

A preliminary combination of this result is made with the search for $T\bar{T} \to Ht + X$, with $H \to b\bar{b}$, that was performed by the ATLAS Collaboration [24] using 14.3 fb^{-1} of data at $\sqrt{s} = 8$ TeV. As mentioned in Section 4, these two searches do not overlap. In the combination, common sources of systematic uncertainty are taken to be fully correlated between both analyses. These include uncertainties on the integrated luminosity, lepton reconstruction, identification and trigger efficiencies, jet identification efficiency, jet energy scale, b, c and light jet tagging efficiencies and theoretical cross sections for backgrounds.

Figure 9 shows the observed and expected upper limits on the $T\bar{T}$ production cross section times branching fraction as a function of m_T for the case of a vector-like singlet T quark. The observed (expected) 95% CL limit is $m_T > 670\,(675)$ GeV for the central value of the theoretical cross section, improving by ~35 GeV the expected sensitivity obtained by the $T\bar{T} \to Ht + X$ analysis. The resulting 95% CL exclusion limits in the two-dimensional branching-ratio plane are shown in Fig. 10 for different values of m_T, significantly expanding the sensitivity compared to the individual analyses. In particular, this combination completely excludes a vector-like T quark with mass in the range of 350–550 GeV, and

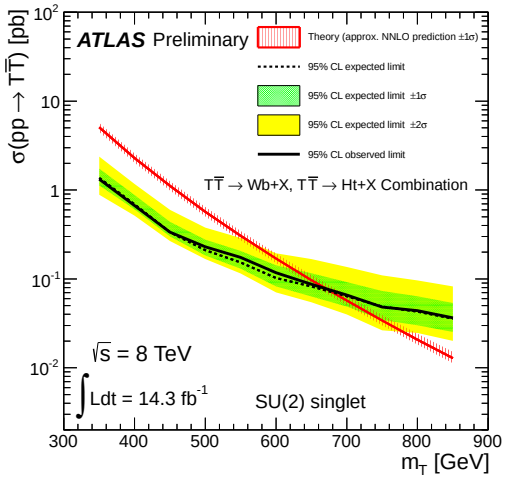

Figure 9: Observed (solid line) and expected (dashed line) 95% CL upper limit on the $T\bar{T}$ cross section times branching fraction for a vector-like singlet T quark as a function of the T quark mass, resulting from the combination of this analysis and that in Ref. [24]. The surrounding shaded bands correspond to the ±1 and ±2 standard deviations around the expected limit. The thin red line and band show the theoretical prediction and its ±1 standard deviation uncertainty.

leaves very little room for a T quark with $m_T = 600$ GeV.

12 Summary

A search has been presented for the production of a heavy top-like quark (T) together with its antiparticle, assuming a significant branching ratio for subsequent decay into a W boson and a b quark. The search is based on 14.3 fb^{-1} of pp collisions at $\sqrt{s} = 8$ TeV recorded in 2012 with the ATLAS detector at the CERN Large Hadron Collider. Data are analysed in the lepton+jets final state, characterised by a high-transverse-momentum isolated electron or muon, large missing transverse momentum and at least four jets, with at least one of them b tagged. The analysis strategy relies on the substantial boost of the W bosons in the $T\bar{T}$ signal when $m_T \gtrsim 400$ GeV. No significant excess of events above the Standard Model expectation is observed. For vector-like T quarks, 95% CL upper limits are derived for various masses in the two-dimensional plane of $BR(T \to Wb)$ versus $BR(T \to Ht)$, where H is the Standard Model Higgs boson. For a vector-like singlet T quark, a mass lower than 505 GeV is excluded at 95% CL. For a chiral fourth generation quark, and under the assumption of a branching ratio $BR(T \to Wb) = 1$, a mass lower than 740 GeV is excluded at 95% CL. The combination with this search with a previous search for $T\bar{T} \to Ht + X$ results in the most restrictive constraints to date on vector-like quarks, completely excluding a vector-like T quark with mass in the range of 350–550 GeV.

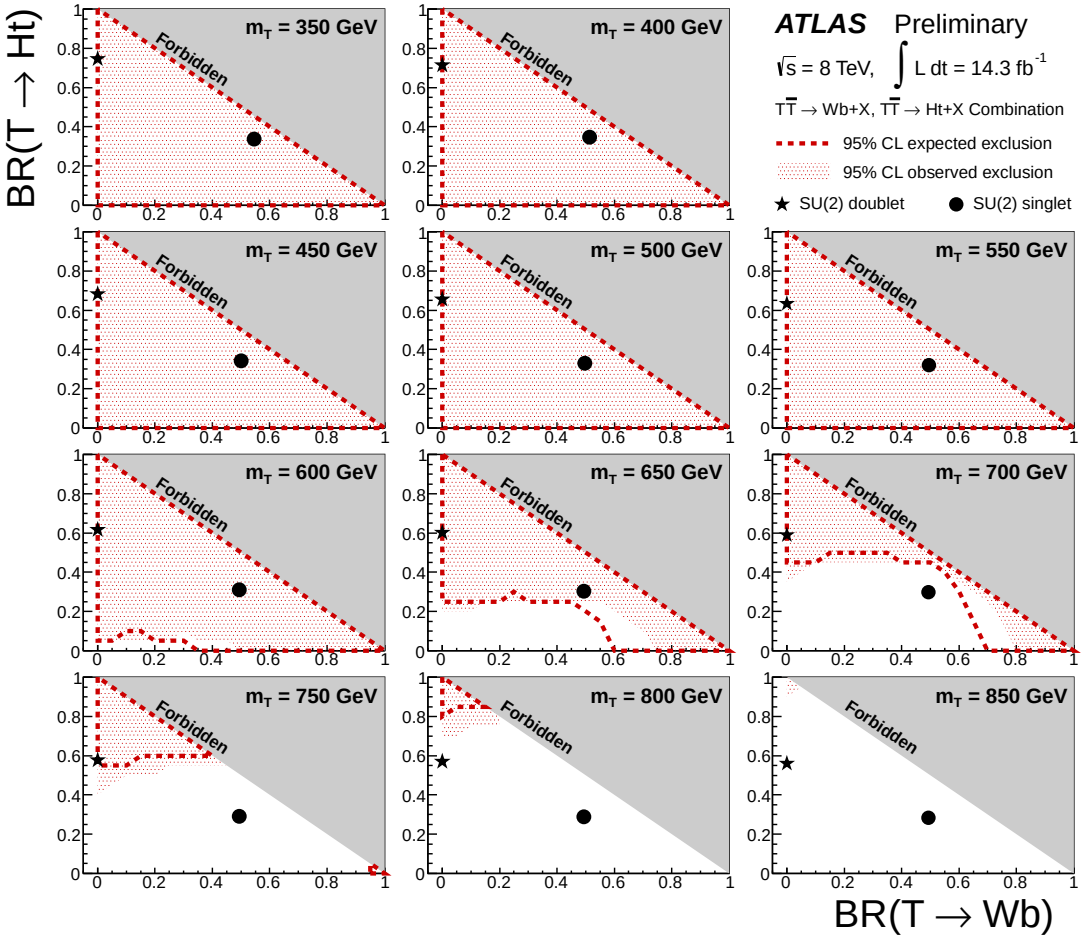

Figure 10: Observed (red filled area) and expected (red dashed line) 95% CL exclusion in the plane of $BR(T \to Wb)$ versus $BR(T \to Ht)$, for different values of the vector-like T quark mass, resulting from the combination of this analysis and that in Ref. [24]. The grey (dark shaded) area corresponds to the unphysical region where the sum of branching ratios exceeds unity. The default branching ratio values from the PROTOS event generator for the weak-isospin singlet and doublet cases are shown as plain circle and star symbols, respectively. This result includes both statistical and systematic uncertainties.

References

[1] CDF Collaboration, F. Abe et al., *Observation of top quark production in $\bar{p}p$ collisions*, Phys. Rev. Lett. **74** (1995) 2626, arXiv:9503002 [hep-ex].

[2] D0 Collaboration, S. Abachi et al., *Observation of the top quark*, Phys. Rev. Lett. **74** (1995) 2632, arXiv:9503003 [hep-ex].

[3] B. Holdom et al., *Four statements about the fourth generation*, PMC Physics A **3** (2009) 4, arXiv:0904.4698 [hep-ph].

[4] S. A. Çetin et al., *Status of the Fourth Generation*, arXiv:1112.2907 [hep-ex].

[5] M. Buchkremer, J.-M. Gérard, and F. Maltoni, *Closing in on a perturbative fourth generation*, JHEP **06** (2012) 135, arXiv:1204.5403 [hep-ph].

[6] ATLAS Collaboration, *Observation of a new particle in the search for the Standard Model Higgs boson with the ATLAS detector at the LHC*, Phys. Lett. B **716** (2012) 1, arXiv:1207.7214 [hep-ex].

[7] CMS Collaboration, *Observation of a new boson at a mass of 125 GeV with the CMS experiment at the LHC*, Phys. Lett. B **716** (2012) 30, arXiv:1207.7235 [hep-ex].

[8] A. Djouadi and A. Lenz, *Sealing the fate of a fourth generation of fermions*, arXiv:1204.1252 [hep-ph].

[9] O. Eberhardt et al., *Impact of a Higgs boson at a mass of* 126 GeV *on the standard model with three and four fermion generations*, Phys. Rev. Lett. **109** (2012) 241802, arXiv:1209.1101 [hep-ph].

[10] J. A. Aguilar-Saavedra, *Identifying top partners at LHC*, JHEP **11** (2009) 030, arXiv:0907.3155 [hep-ph].

[11] N. Arkani-Hamed, A. G. Cohen, and H. Georgi, *Electroweak symmetry breaking from dimensional deconstruction*, Phys. Lett. B **513** (2001) 232, arXiv:0105239 [hep-ph].

[12] N. Arkani-Hamed, A. Cohen, E. Katz, and A. Nelson, *The Littlest Higgs*, JHEP **0207** (2002) 034, arXiv:0206021 [hep-ph].

[13] M. Perelstein, *Little Higgs Models and Their Phenomenology*, Prog. Part. Nucl. Phys. **58** (2007) 247, arXiv:0512128 [hep-ph].

[14] R. Contino, L. D. Rold, and A. Pomarol, *Light custodians in natural composite Higgs models*, Phys. Rev. D **75** (2007) 055014, arXiv:0607106 [hep-ph].

[15] M. Carena, E. Ponton, J. Santiago, and C. E. Wagner, *Light Kaluza-Klein States in Randall-Sundrum Models with Custodial SU(2)*, Nucl. Phys. **B 759** (2006) 202, arXiv:0607106 [hep-ph].

[16] D. Choudhury, T. M. P. Tait, and C. E. M. Wagner, *Beautiful mirrors and precision electroweak data*, Phys. Rev. D **65** (2002) 053002, arXiv:0109097 [hep-ph].

[17] B. Batell, S. Gori, and L. T. Wang, *Higgs Couplings and Precision Electroweak Data*, JHEP **01** (2013) 139, arXiv:1209.6382 [hep-ph].

[18] J. A. Aguilar-Saavedra, R. Benbrik, S. Heinemeyer, and M. Perez-Victoria, *A handbook of vector-like quarks: mixing and single production*, arXiv:1306.0572 [hep-ph].

[19] ATLAS Collaboration, *Search for pair production of heavy top-like quarks decaying to a high-p_{T} W boson and a b quark in the lepton plus jets final state at $\sqrt{s}$ = 7 TeV with the ATLAS detector*, Phys. Lett. **B718** (2013) 1284, arXiv:1210.5468 [hep-ex].

[20] CMS Collaboration, *Search for pair produced fourth-generation up-type quarks in pp collisions at $\sqrt{s}$ = 7 TeV with a lepton in the final state*, Phys. Lett. **B718** (2012) 307, arXiv:1209.0471 [hep-ex].

[21] ATLAS Collaboration, *Search for pair-produced heavy quarks decaying to Wq in the two-lepton channel at $\sqrt{s}$ = 7 TeV with the ATLAS detector*, Phys. Rev. D **86** (2012) 012007, arXiv:1202.3389 [hep-ex].

[22] CMS Collaboration, *Search for heavy, top-like quark pair production in the dilepton final state in pp collisions at $\sqrt{s}$ = 7 TeV*, Phys. Lett. **B716** (2012) 103, arXiv:1203.5410 [hep-ex].

[23] CMS Collaboration, *Search for heavy quarks decaying into a top quark and a W or Z boson using lepton + jets events in pp collisions at $\sqrt{s}$ = 7 TeV*, JHEP **01** (2013) 154, arXiv:1210.7471 [hep-ex].

[24] ATLAS Collaboration, *Search for heavy top-like quarks decaying to a Higgs boson and a top quark in the lepton plus jets final state in pp collisions at $\sqrt{s}$ = 8 TeV with the ATLAS detector*, ATLAS-CONF-2013-018 (2013) . https://cds.cern.ch/record/1525525.

[25] B. Holdom, *t' at the LHC: the physics of discovery*, JHEP **03** (2007) 063, arXiv:0702037v3 [hep-ph].

[26] B. Holdom, *The heavy quark search at the LHC*, JHEP **08** (2007) 069, arXiv:0705.1736v1 [hep-ph].

[27] B. Holdom, *Approaching a strong fourth family*, Phys. Lett. B **686** (2010) 146, arXiv:1001.5321v2 [hep-ph].

[28] ATLAS Collaboration, *The ATLAS Experiment at the CERN Large Hadron Collider*, JINST **3** (2008) S08003.

[29] ATLAS Collaboration, *Electron performance measurements with the ATLAS detector using the 2010 LHC proton-proton collision data*, Eur. Phys. J. C **72** (2012) 1909, arXiv:1110.3174 [hep-ex].

[30] M. Cacciari, G. P. Salam, and G. Soyez, *The anti-k_t jet clustering algorithm*, JHEP **04** (2008) 063, arXiv:0802.1189v2 [hep-ph].

[31] M. Cacciari and G. P. Salam, *Dispelling the N^3 myth for the k_t jet-finder*, Phys. Lett. **B641** (2006) 57, arXiv:0512210v2 [hep-ph].

[32] M. Cacciari, G. P. Salam, and G. Soyez, *FastJet User Manual*, Eur. Phys. J. **C72** (2012) 1896, arXiv:1111.6097 [hep-ph].

[33] C. Cojocaru et al., *Hadronic calibration of the ATLAS liquid argon end-cap calorimeter in the pseudorapidity region* $1.6 < |\eta| < 1.8$ *in beam tests*, Nucl. Instr. Meth. A **531** (2004) 481, arXiv:0407009 [physics].

[34] T. Barillari et al., *Local hadronic calibration*, ATL-LARG-PUB-2009-001 (2009) . https://cds.cern.ch/record/1112035.

[35] ATLAS Collaboration, ATLAS Collaboration, *Jet energy measurement with the ATLAS detector in proton-proton collisions at* $\sqrt{s}$ = 7 TeV, Eur. Phys. J. C **73** (2013) 2304, arXiv:1112.6426 [hep-ex].

[36] ATLAS Collaboration, *Commissioning of the ATLAS high-performance b-tagging algorithms in the 7 TeV collision data*, ATLAS-CONF-2011-102 (2011) . https://cds.cern.ch/record/1369219.

[37] ATLAS Collaboration, *Reconstruction and Calibration of Missing Transverse Energy and Performance in Z and W events in ATLAS Proton-Proton Collisions at 7 TeV*, ATLAS-CONF-2011-080 (2011) . https://cds.cern.ch/record/1355703.

[38] ATLAS Collaboration, *Measurement of the top quark-pair production cross section with ATLAS in pp collisions at* $\sqrt{s}$ = 7 TeV, Eur. Phys. J. C **71** (2011) 1577, arXiv:1012.1792 [hep-ex].

[39] ATLAS Collaboration, *Measurement of the charge asymmetry in top quark pair production in pp collisions at* $\sqrt{s}$ = 7 TeV *using the ATLAS detector*, Eur. Phys. J. C **72** (2012) 2039, arXiv:1203.4211 [hep-ex].

[40] S. Frixione and B. R. Webber, *Matching NLO QCD computations and parton shower simulations*, JHEP **06** (2002) 029, arXiv:0204244 [hep-ph].

[41] S. Frixione, E. Laenen, P. Motylinski, and B. R. Webber, *Single-top production in MC@NLO*, JHEP **03** (2006) 092, arXiv:0512250 [hep-ph].

[42] S. Frixione, E. Laenen, P. Motylinski, C. White, and B. R. Webber, *Single-top hadroproduction in association with a W boson*, JHEP **07** (2008) 029, arXiv:0805.3067 [hep-ph].

[43] H.-L. Lai et al., *New parton distributions for collider physics*, Phys. Rev. D **82** (2010) 074024, arXiv:1007.2241 [hep-ph].

[44] B. P. Kersevan and E. Richter-Was, *The Monte Carlo Event Generator AcerMC 2.0 with Interfaces to PYTHIA 6.2 and HERWIG 6.5*, arXiv:0405247 [hep-ph].

[45] A. Sherstnev and R. Thorne, *Parton distributions for LO generators*, Eur. Phys. J. C **55** (2008) 553, arXiv:0711.2473 [hep-ph].

[46] G. Corcella et al., *HERWIG 6: an event generator for hadron emission reactions with interfering gluons (including supersymmetric processes)*, JHEP **01** (2001) 010.

[47] T. Sjostrand et al., *High-energy-physics event generation with Pythia 6.1*, Comput. Phys. Commun. **135** (2001) 238, arXiv:0010017 [hep-ph].

[48] M. Aliev et al., *HATHOR: a Hadronic Top and Heavy quarks cross section calculator*, Comput. Phys. Commun. **182** (2011) 1034, arXiv:1007.1327 [hep-ph].

[49] N. Kidonakis, *Next-to-next-to-leading-order collinear and soft gluon corrections for t-channel single top quark production*, Phys. Rev. D **83** (2011) 091503, arXiv:1103.2792 [hep-ph].

[50] N. Kidonakis, *Two-loop soft anomalous dimensions for single top quark associated production with a* W^- *or* H^-, Phys. Rev. D **82** (2010) 054018, arXiv:1005.4451 [hep-ph].

[51] N. Kidonakis, *Next-to-next-to-leading logarithm resummation for s-channel single top quark production*, Phys. Rev. D **81** (2010) 054028, arXiv:1001.5034 [hep-ph].

[52] A. D. Martin et al., *Parton distributions for the LHC*, Eur. Phys. J. C **63** (2009) 189, arXiv:0901.0002 [hep-ph].

[53] A. D. Martin et al., *Uncertainties on α_S in global PDF analyses and implications for predicted hadronic cross sections*, Eur. Phys. J. C **64** (2009) 653, arXiv:0905.3531 [hep-ph].

[54] M. L. Mangano et al., *ALPGEN, a generator for hard multiparton processes in hadronic collisions*, JHEP **07** (2003) 001, arXiv:0206293 [hep-ph].

[55] P. M. Nadolsky et al., *Implications of CTEQ global analysis for collider observables*, Phys. Rev. D **78** (2008) 013004, arXiv:0802.0007 [hep-ph].

[56] M. L. Mangano et al., *Multijet matrix elements and shower evolution in hadronic collisions: $Wb\bar{b}$ + n jets as a case study*, Nucl. Phys. **B 632** (2002) 343, arXiv:0108069 [hep-ph].

[57] ATLAS Collaboration, *Measurement of the t-channel single top-quark production cross section in pp collisions at $\sqrt{s}$ = 7 TeV with the ATLAS detector*, Phys. Lett. **B717** (2012) 330, arXiv:1205.3130 [hep-ex].

[58] K. Melnikov and F. Petriello, *Electroweak gauge boson production at hadron colliders through $O(\alpha_s^2)$*, Phys. Rev. D **74** (2006) 114017, arXiv:0609070 [hep-ph].

[59] J. Campbell and R. Ellis, *An update on vector boson pair production at hadron colliders*, Phys. Rev. D **60** (1999) 113006, arXiv:9905386 [hep-ph].

[60] J. Alwall et al., *MadGraph/MadEvent v4: the new web generation*, JHEP **09** (2007) 028, arXiv:0706.2334 [hep-ph].

[61] J. M. Campbell and R. K. Ellis, *$t\bar{t}W$ production and decay at NLO*, arXiv:1204.5678 [hep-ph].

[62] M. V. Garzelli, A. Kardos, C. G. Papadopoulos, and Z. Trcsnyi, *$t\bar{t}W$ and $t\bar{t}Z$ Hadroproduction at NLO accuracy in QCD with Parton Shower and Hadronization effects*, JHEP **1211** (2012) 056, arXiv:1208.2665 [hep-ph].

[63] LHC Higgs Cross Section Working Group Collaboration, S. Dittmaier et al., *Handbook of LHC Higgs Cross Sections: 1. Inclusive Observables*, arXiv:1101.0593 [hep-ph].

[64] J. A. Aguilar-Saavedra, *PROTOS, a Program for Top Simulations*, . http://jaguilar.web.cern.ch/jaguilar/protos/.

[65] A. Djouadi, J. Kalinowski, and M. Spira, *HDECAY: a Program for Higgs Boson Decays in the Standard Model and its Supersymmetric Extension*, Comput. Phys. Commun. **108** (1998) 56, arXiv:9704448 [hep-ph].

[66] J. Butterworth, J. Forshaw, and M. Seymour, *Multiparton interactions in photoproduction at HERA*, Z. Phys. C **72** (1996) 637, arXiv:9601371 [hep-ph].

[67] P. Golonka and Z. Wąs, *PHOTOS Monte Carlo: a precision tool for QED corrections in Z and W decays*, Eur. Phys. J. C **45** (2006) 97, arXiv:0506026 [hep-ph].

[68] S. Jadach, J. H. Kühn, and Z. Waąs, *TAUOLA - a library of Monte Carlo programs to simulate decays of polarized τ leptons*, Comput. Phys. Commun. **64** (1991) 275.

[69] ATLAS Collaboration, *The ATLAS Simulation Infrastructure*, Eur. Phys. J. C **70** (2010) 823, arXiv:1005.4568 [physics.ins-det].

[70] S. Agostinelli et al., *Geant4: a simulation toolkit*, Nucl. Instr. Meth. A **506** (2003) 250.

[71] ATLAS Collaboration, *Measurements of top quark pair relative differential cross sections with ATLAS in pp collisions at $\sqrt{s}$ = 7 TeV*, Eur. Phys. J. C **73** (2013) 2261, arXiv:1207.5644 [hep-ex].

[72] ATLAS Collaboration, *Luminosity determination in pp collisions at $\sqrt{s}$ = 7 TeV using the ATLAS detector at the LHC*, Eur. Phys. J. C **71** (2011) 1630, arXiv:1101.2185 [hep-ex].

[73] ATLAS Collaboration, *In-situ jet pseudorapidity intercalibration of the ATLAS detector using dijet events in $\sqrt{s}$ = 7 TeV proton-proton 2011 data*, ATLAS-CONF-2012-124 (2012) . http://cds.cern.ch/record/1474490.

[74] ATLAS Collaboration, *Pile-up corrections for jets from proton-proton collisions at $\sqrt{s}$ = 7 TeV in ATLAS in 2011*, ATLAS-CONF-2012-064 (2012) . http://cds.cern.ch/record/1459529.

[75] ATLAS Collaboration, *JES uncertainties for 2012 data*, . https://twiki.cern.ch/twiki/bin/view/AtlasPublic/JetEtmissApproved2013JESUncertainty.

[76] ATLAS Collaboration, *Measurement of the b-tag Efficiency in a Sample of Jets Containing Muons with 5 fb^{-1} of Data from the ATLAS Detector*, ATLAS-CONF-2012-043 (2012) . https://cds.cern.ch/record/1435197.

[77] ATLAS Collaboration, *b-jet tagging calibration on c-jets containing D^* mesons*, ATLAS-CONF-2012-039 (2012) . https://cds.cern.ch/record/1435193.

[78] ATLAS Collaboration, *Measurement of the Mistag Rate of b-tagging algorithms with 5 fb^{-1} of Data Collected by the ATLAS Detector*, ATLAS-CONF-2012-040 (2012) . https://cds.cern.ch/record/1435194.

[79] ATLAS Collaboration, *Measurement of $t\bar{t}$ production with a veto on additional central jet activity in pp collisions at $\sqrt{s}$ = 7 TeV using the ATLAS detector*, Eur. Phys. J. C **72** (2012) 2043, arXiv:1203.5015 [hep-ex].

[80] T. Junk, *Confidence level computation for combining searches with small statistics*, Nucl. Instr. Meth. A **434** (1999) 435, arXiv:9902006 [hep-ex].

[81] A. L. Read, *Presentation of search results: the CL_s technique*, J. Phys. G **28** (2002) 2693.